J. Fluid Mech. (1994), *vol.* 279, *pp.* 169–176

Hyperviscous vortices

By JAVIER JIMÉNEZ
School of Aeronautics, Pl. Cardenal Cisneros 3, 28040 Madrid, Spain

(Received 3 February 1994 and in revised form 18 May 1994)

The structure of diffusing planar and axisymmetric vortices of the hyperviscous Navier–Stokes equations is studied for different orders of the dissipative operator. It is found that, except for the classical Newtonian case, the vorticity decays at large distances by means of oscillatory tails, containing circulation of alternating signs. This oscillation becomes stronger for large hyperviscosity orders, and the limit of infinite order is studied. It is argued that these solutions would become unstable for large enough Reynolds numbers, and may contribute non-trivial spurious dynamics to flow simulations using hyperviscosity.

1. Introduction

Hyperviscosity, the substitution of higher iterations of the Laplacian, ∇^{2n}, for the second-order dissipative operator of the Navier–Stokes equations, has been used often in the numerical simulation of turbulent flows to extend the range of the inviscid inertial cascade which can be achieved with a given resolution. The hyperviscosity order is chosen in most cases as $n = 2$ (Santangelo, Benzi & Legras 1989; McWilliams 1990; Ohkitani 1991; Nakamura, Takahashi & Nakano 1993) but is occasionally pushed to higher values, $n = 8$ (Babiano *et al.* 1987; Borue 1993; Maltrud & Vallis 1993; Smith & Yakhot 1993). While it is usually stated that the choice of the dissipation mechanism does not have a strong influence on the physics of the inertial range (Santangelo *et al.* 1989), it is conceivable that the different equations might have unexpected secondary effects on the flow and that, in particular, they may result in a different balance of convective and viscous terms in the crossover spectral range at the near-dissipative scales (Maltrud & Vallis 1993). Since it has been documented that this range is dominated, or at least characterized, by the presence of compact vorticity structures, both in two-dimensional (Fornberg 1977; McWilliams 1984; Dritschel 1993 and references therein) and in three-dimensional turbulent flows (Kuo & Corrsin 1972; Siggia 1981; Jiménez *et al.* 1993 and references therein), it may be of some interest to study how these structures are affected by the use of different orders of hyperviscosity. Moreover, once this is done, it may be possible to learn more about the significance of those compact structures in natural Newtonian flows by purposely introducing dissipation of different orders in numerical simulations of turbulence and by observing the resulting changes.

In this paper we study the structure of isolated hyperviscous vorticity structures, both planar and axisymmetric. In the next section we present solutions for the planar vortex sheet, valid both for the limit of self-similar hyperviscous spreading and for the state of equilibrium between diffusion and a plane strain. The equivalent axisymmetric problem is studied in §3, followed in §4 by some discussion of stability and by a numerical example.

2. The planar vortex sheet

Consider the Navier–Stokes equations for an incompressible hyperviscous fluid

$$\left.\begin{aligned} \partial_t \boldsymbol{u} + \boldsymbol{u}\cdot\boldsymbol{\nabla}\boldsymbol{u} + \boldsymbol{\nabla} p &= \nu(-\Delta)^n \boldsymbol{u}, \\ \boldsymbol{\nabla}\cdot\boldsymbol{u} &= 0, \end{aligned}\right\} \tag{1}$$

where ν is a hyperviscosity coefficient which should be positive to ensure well-posedness of the equations. We define n as the *order* of the hyperviscosity operator. In this paper we assume it to be an integer, although in a pseudospectral simulation code, where the Laplacian is substituted by the square of the wavenumber magnitude, it could be an arbitrary real number. That extra freedom may be useful in some cases to study the evolution of flow properties with the order of hyperviscosity.

One of the simplest solutions to those equations is a diffusing vortex layer driven by a uniform plane strain,

$$u = -\alpha x, \quad v = 0, \quad w = \alpha z, \tag{2}$$

in which the flow is assumed to depend only on the coordinate x, except for the driving velocity. We will use from now on dimensionless quantities, although the normalization will vary for the different cases. In the definition of the normalizations, the dimensionless variables will be denoted by primes, but those primes will be left out of the equations themselves. With this convention, the equation for the collapsing vortex layer becomes

$$\partial_t \omega - \partial_x(x\omega) + (-1)^n \partial_x^{2n} \omega = 0, \tag{3}$$

where ω is the only non-zero component of the vorticity, directed along the z-axis, and the dimensionless variables are defined as

$$x' = x(\alpha/\nu)^{1/2n}, \quad t' = \alpha t, \quad \omega' = \omega/\alpha. \tag{4}$$

We will be specially interested in the steady Burgers' sheet, which is the long-time limit of the solution to (3) with the vorticity decaying to zero as $x \to \pm\infty$.

The same equation is relevant to the two-dimensional case in which the vortex layer spreads by diffusion without any driving strain. The appropriate 'similarity' variables are

$$x' = x/(2n\nu t)^{1/2n}, \quad t' = (1/2n)\log t, \quad \omega = t^{-1/2n}\omega'(x', t'), \tag{5}$$

and the resulting vorticity equation is identical to (3). The interesting solution is then the self-similar spreading layer in which the normalized vorticity is independent of t'.

A first idea of the character of the steady solutions to (3) can be obtained from the WKB approximation to their behaviour at large $|x|$. Consider $x > 0$ and substitute (see e.g. Bender & Orszag 1978, pp. 484–497)

$$\omega \sim \exp\left[S_0(x) + S_1(x) + \cdots\right], \quad S_0 \gg S_1 \gg \cdots, \quad S_0 \gg 1. \tag{6}$$

Equating comparable terms we obtain the eikonal equation

$$(\mathrm{d}S_0/\mathrm{d}x)^{2n-1} = (-1)^n x, \tag{7}$$

which has $2n-1$ solutions,

$$S_0 = \frac{2n-1}{2n}\sigma x^{2n/(2n-1)}, \quad \sigma^{2n-1} = (-1)^n, \tag{8}$$

which are distinguished by the $2n-1$ complex roots σ. The lowest-order WKB approximation takes the form

$$\omega \sim x^{(1-n)/(2n-1)} \exp\left[\frac{2n-1}{2n}\sigma x^{2n/(2n-1)}\right]. \tag{9}$$

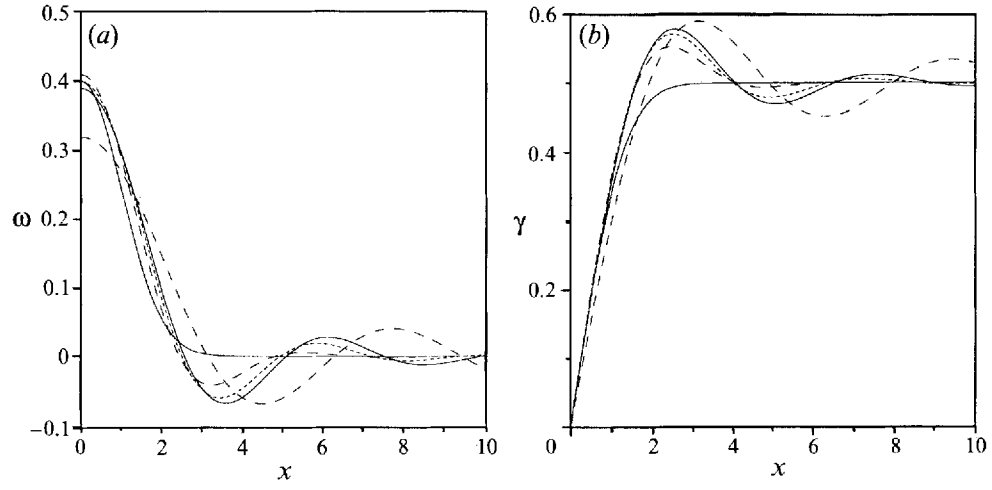

FIGURE 1. Vorticity distributions for planar diffusing vortex sheets with different orders of hyperviscosity. In order of increasing oscillation amplitude, $n = 1, 2, 3, 4, \infty$. (*a*) Vorticity. (*b*) Integrated circulation from plane of symmetry, $\gamma(x) = \int_0^x \omega(x)\,\mathrm{d}x$.

Of these solutions the only relevant ones are those for which the real part of σ is negative, so that the exponential factor decays as x increases. There are in general n such solutions, corresponding to $\lfloor n/2 \rfloor$ pairs of complex σ, plus one solution with $\sigma = -1$ if n is odd. It is interesting that, except for the Newtonian case of $n = 1$, some of the solutions correspond to complex σ, and decay at infinity with oscillatory tails containing vorticity of both signs. The classical viscous layer, with a Gaussian vorticity distribution (Batchelor 1967, pp. 272–273), is the only one whose tails decay to zero monotonically.

For each hyperviscosity order there is a single family of solutions satisfying the condition that the vorticity vanishes at infinity. To show that this is true, we need to find conditions that determine a unique linear combination of the n acceptable WKB solutions. From the symmetry of the driving flow we can assume that the solution itself is symmetric around $x = 0$, so that all the odd derivatives of ω vanish at the origin. This assumption will be justified later, and supplies $n-1$ conditions to fix all but one of the coefficients needed. The remaining one is an amplitude scale that is given by the total (conserved) circulation per unit sheet area,

$$\gamma = \int_{-\infty}^{\infty} \omega(x)\,\mathrm{d}x. \tag{10}$$

The numerical solution for several hyperviscosity orders, with $\gamma = 1$, is shown in figure 1 (*a*). It is seen that oscillations are present for all but the Newtonian case, and that they become stronger as the order increases. It also follows from (8) that the decay of the vorticity in the tails becomes increasingly exponential as n increases, in contrast to the Gaussian decay for $n = 1$.

It is of some interest to understand the limiting behaviour of the solutions in the 'ultraviscosity' case $n \to \infty$. In this limit the numerical solution becomes difficult, but a different representation is useful. Consider the Fourier transform of ω,

$$\Omega(k, t) = \frac{1}{2\pi} \int_{-\infty}^{\infty} \omega(x, t)\, \mathrm{e}^{-\mathrm{i}kx}\,\mathrm{d}x. \tag{11}$$

Equation (11) can be transformed into

$$\partial_t \Omega + k\partial_k \Omega + k^{2n}\Omega = 0, \tag{12}$$

which is hyperbolic in (k, t), with characteristics given by

$$\mathrm{d}k/\mathrm{d}t = k, \quad k = k_0\, \mathrm{e}^t, \tag{13}$$

along which the equation can be written as an ordinary differential equation and integrated directly as

$$k\frac{\mathrm{d}\Omega}{\mathrm{d}k} + k^{2n}\Omega = 0, \quad \Omega(k,t) = \Omega(k_0, 0)\exp\left[(k_0^{2n} - k^{2n})/2n\right]. \tag{14}$$

As $t \to \infty$, it follows from (13) that $k_0 \to 0$ for any fixed k, and the Fourier transform of the asymptotic steady solution is given by

$$\Omega(k) = \Omega(0,0)\exp\left(-k^{2n}/2n\right) = \frac{\gamma}{2\pi}\exp\left(-k^{2n}/2n\right). \tag{15}$$

Note that this procedure results directly in a unique solution, which appears as the long-time limit of the initial value problem. The fact that the Fourier transform in (15) is real shows that the solution obtained in this way is symmetric with respect to $x = 0$. This solution is selected because the process by which the transformed equation (12) was obtained assumes implicitly that the solution decays at $x \to \pm\infty$ fast enough for a continuous Fourier transform to exist everywhere on the real axis. In fact, the solution can be expressed as a Fourier integral

$$\omega(x) = 2\int_0^\infty \cos(kx)\,\Omega(k)\,\mathrm{d}k. \tag{16}$$

For $n = 1$ it follows from (15) that the spectrum is Gaussian, and so is the solution, in agreement with the classical result. In the ultraviscosity limit, the Fourier transform becomes a step function, constant below the Burgers' scale $|k| \leqslant 1$, and falling abruptly to zero beyond it. Direct substitution in (16) provides the solution,

$$\omega_\infty(x) = \gamma \sin(x)/\pi x, \tag{17}$$

which is included in figure 1 for comparison. In figure 1 (*b*) we show the circulation contained between the plane of symmetry and a given x. It is seen that the oscillations in the tail contain a substantial fraction of the total circulation of the layer, even for the lowest hyperviscosity order, $n = 2$, raising the question of whether the alternating sign of the vorticity would become important in numerical simulations of turbulence, inducing, for example, spurious instabilities in the interaction between structures.

3. Axisymmetric vortices

The axisymmetric case can be treated similarly to the planar sheet. Consider first the steady Burgers' vortex, driven by an axial strain

$$u_z = \alpha z, \quad u_r = -\tfrac{1}{2}\alpha r. \tag{18}$$

We will assume that the distribution of axial vorticity varies only radially and is independent of the axial coordinate z, and that all the other vorticity components are zero. The normalized vorticity equation is

$$\partial_t \omega - (1/r)\,\partial_r(r^2\omega) + (-\Delta)^n\omega = 0, \tag{19}$$
$$\Delta = (1/r)\,\partial_r(r\,\partial_r),$$

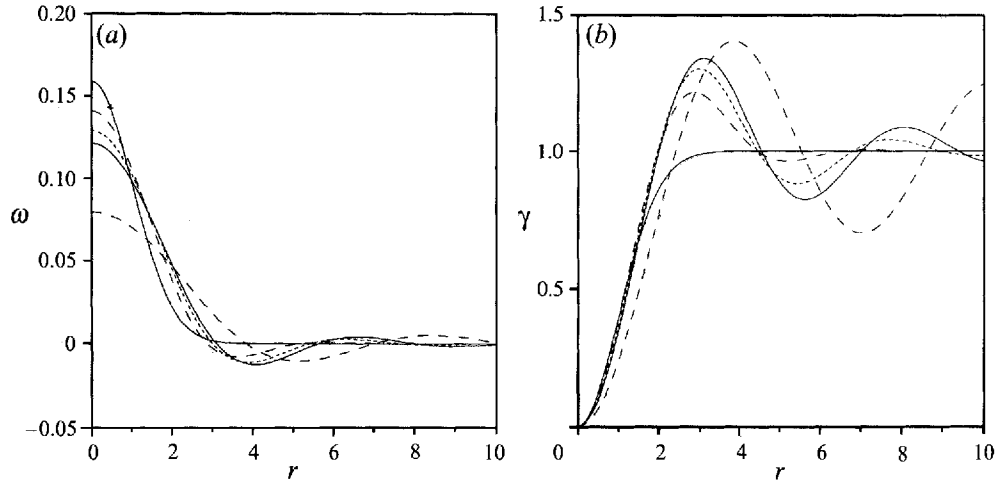

FIGURE 2. Vorticity distributions for axisymmetric diffusing vortices with different orders of hyperviscosity. In order of decreasing vorticity at the axis, $n = 1, 2, 3, 4, \infty$. (*a*) Vorticity. (*b*) Integrated circulation from axis, $\gamma(r) = 2\pi \int_0^r r\omega(r)\,\mathrm{d}r$.

where the normalized radius is defined as

$$r' = r(\alpha/2\nu)^{1/2n}, \tag{20}$$

while the dimensionless time and vorticity are as in (4). As in the case of the vortex sheet, the equation for the decay of an axisymmetric vortex, without a driving strain, can be put into the form (19) by a transformation similar to (5),

$$r' = r/(n\nu t)^{1/2n}, \quad t' = (1/n)\log t, \quad \omega = t^{-1/n}\omega'(r', t'). \tag{21}$$

The behaviour of the vorticity at large radius is obtained as before, and the eikonal equation is identical in both cases. The leading approximation is

$$\omega \sim r^{1/(2n-1)} \exp\left[\frac{2n-1}{2n}\sigma r^{2n/(2n-1)}\right], \tag{22}$$

where σ is the same multiple root as above. The presence and character of the tail oscillations are therefore also identical. As in the previous case, there is a unique family of continuous solutions for each order, decaying to zero at infinity. The necessary conditions are now that all the odd radial derivatives vanish at the axis, plus the given circulation per unit axial length. Figure 2(*a*, *b*) gives some examples of solutions for different orders. The tail oscillations now appear milder than in the planar case, but the amount of circulation that they contain is similar.

The ultraviscosity limit can also be studied by spectral methods. The two-dimensional Fourier transform of an axisymmetric function depends only of the modulus of the wavenumber vector, $k = (k_x^2 + k_y^2)^{1/2}$, and can be expressed as a one-dimensional integral, known as the Hankel transform (e.g. Carrier, Krook & Pearson 1966, pp. 366–367)

$$\Omega(k) = \frac{1}{2\pi}\int_0^\infty r\omega(r)\,J_0(kr)\,\mathrm{d}r, \tag{23}$$

where J_0 is the zeroth-order Bessel function of the first kind. The properties of this transform are similar to those of the classical Fourier formula, of which it is just a

particular formulation. In fact, the transform of (19) is (12), as in the planar case, and we conclude immediately that the Hankel transform of the solution is also identical, although with a different normalization factor in terms of the circulation

$$\Omega(k) = \frac{\gamma}{4\pi^2} \exp(-k^{2n}/2n). \tag{24}$$

The Hankel transform can be inverted to obtain a general quadrature expression for the vorticity,

$$\omega(r) = 2\pi \int_0^\infty k\Omega(k) J_0(kr)\, \mathrm{d}k, \tag{25}$$

which, as $n \to \infty$ and the spectrum tends to a step function, approaches the ultraviscosity limit

$$\omega_\infty(r) = \gamma J_1(r)/2\pi r. \tag{26}$$

This solution has been included in figure 2 for comparison.

4. Discussion

The most striking characteristic of the solutions discussed here is the presence of vorticity of opposite sign in the periphery of the main structure. Even if these are solutions dominated by diffusion, the Reynolds number based on the tangential velocity is not necessarily small, and inviscid instabilities may become important if it is chosen large enough. The consequences are different for the different flows. In the case of the planar sheet, the sheet itself is unstable to Kelvin–Helmholtz instabilities, and the presence of an extra instability in the weaker layer of vorticity of opposite sign is probably not important by comparison.

The axisymmetric case is different. A circular vortex is stable to two-dimensional perturbations as long as the radial distribution of vorticity is monotonic, but may become unstable otherwise (Rayleigh 1880). This is essentially again the Kelvin–Helmholtz instability and takes the form of azimuthal waves which reach their maximum intensity at the radial location where the vorticity reaches an extremum which, in this case, would be the first vorticity minimum at the periphery. Eventually, these waves would saturate at an amplitude which is a low multiple of the maximum vorticity of the unstable layer, which is itself a few percent of the maximum vorticity of the main vortex. These waves are weak compared to the main vortex but, as noted above, contain a substantial circulation, and may modify, for example, the interaction of vortices in two-dimensional simulations of turbulence.

Another example of non-trivial dynamics due to the spurious vorticity generated by hyperviscosity is shown in figure 3, which displays four snapshots of a periodic array of vortices of the same sign, diffusing under hyperviscosity with $n = 2$. A weak band of negative vorticity appears on either side of the array, and develops waves which travel with a velocity close to that of the free stream at infinity. Even if the intensity of the negative vorticity is only 2–3% of the maximum vorticity at the centre of the vortices, the presence of the wave is enough to induce a visible perturbation in their shape. In this particular case, and with the periodicity imposed by the numerical scheme, the flow decays to a uniform vortex layer like the one analysed in §2. In a computation with unlimited horizontal periodicity the initial vortex array would be unstable to pairing, and that instability would probably be triggered sooner by the spurious vorticity waves on the periphery.

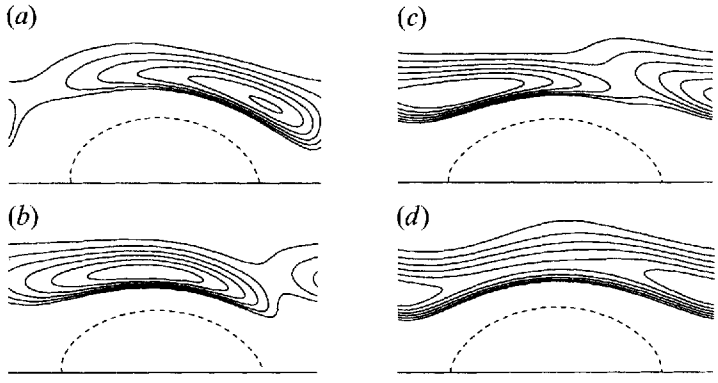

FIGURE 3. Vorticity maps for the simulation described in text. Circulation of each vortex: $\gamma = 25$. Wavelength: $\Delta x = 2\pi$. $\nu = 0.0025$. Negative isolines, solid: $\omega = -0.11$, -0.01, (0.02). Positive isoline, dashed: $\omega = 1$. Maximum vorticity at vortex centre: $\omega \approx 5$. Time between consecutive frames, (*a*)–(*d*): $\Delta t = 1$. Numerical scheme is fully spectral, 256^2 modes, with vertical boundary conditions mapped to infinity. Each map contains the upper half of a full wavelength.

Other instabilities are possible, although their influence on the behaviour of the main vortex is also likely to be limited. For example, if we consider columnar, rather than two-dimensional vortices, the fact that the circulation decreases locally at their periphery (figure 2*b*) would make them subject to centrifugal instabilities (Rayleigh 1880).

An interesting property of the hyperviscous solutions is the sharpness of their spectral cutoff, which goes from a smooth Gaussian fall-off for Newtonian viscosity, to a step function in the ultraviscosity limit. This is in agreement with the intuitive effect of hyperviscosity and, although there is no clear relation between spectral characteristics and dynamics, the presence of the cutoff may be useful in diagnosing the presence and relative weight of the different types of structures in turbulent simulations. A more disturbing possibility is that the presence of the negative vorticity might have global effects on the hyperviscous calculations of two-dimensional turbulence, specially in those using higher orders. It was shown in Dritschel (1993) that turbulence calculations using a dissipation model different from viscosity behave differently in some respects from those in McWilliams (1990), which use hyperviscosity with $n = 2$. While it is not clear in that particular case how much of the effect is due to numerical artifacts, it strengthens the argument that details of the dissipation mechanism may influence bulk properties of turbulence, and that hyperviscosity might not be an altogether benign way of increasing the inertial range of turbulent flows.

This work was partially supported by the Human Capital and Mobility program of the EEC under contract ERBCHRXCT920001.

REFERENCES

BABIANO, A., BASDEVANT, C., LEGRAS, B. & SADOURNY, R. 1987 Vorticity and passive scalar dynamics in two-dimensional turbulence. *J. Fluid Mech.* **183**, 379–397.

BATCHELOR, G. K. 1967 *An introduction to Fluid Dynamics.* Cambridge University Press.

BENDER, C. M. & ORSZAG, S. A. 1978 *Advanced Mathematical Methods for Scientists and Engineers.* McGraw Hill.

BORUE, V. 1993 Spectral exponents of enstrophy cascade in stationary two-dimensional homogeneous turbulence. *Phys. Rev. Lett.* **71**, 3967–3970.

CARRIER, C. F., KROOK, M. & PEARSON, C. E. 1966 *Functions of Complex Variables*. McGraw-Hill.

DRITSCHEL, D. G. 1993 Vortex properties of two-dimensional turbulence. *Phys. Fluids* A **5**, 984–997.

FORNBERG, B. 1977 A numerical study of 2-D turbulence. *J. Comput. Phys.* **25**, 1–31.

JIMÉNEZ, J., WRAY, A., SAFFMAN, P. G. & ROGALLO, R. S. 1993 The structure of intense vorticity in isotropic turbulence. *J. Fluid Mech.* **255**, 65–90.

KUO, A. Y. & CORRSIN, S. 1972 Experiments on the geometry of the fine-structure regions in fully turbulent fluid. *J. Fluid Mech.* **56**, 447–479.

MALTRUD, M. E. & VALLIS, G. K. 1993 Energy and enstrophy transfer in numerical simulations of two-dimensional turbulence. *Phys. Fluids* A **5**, 984–997.

MCWILLIAMS, J. C. 1984 The emergence of isolated coherent vortices in turbulent flows. *J. Fluid Mech.* **146**, 21–43.

MCWILLIAMS, J. C. 1990 The vortices of two-dimensional turbulence. *J. Fluid Mech.* **219**, 361–385.

NAKAMURA, K., TAKAHASHI, T. & NAKANO, T. 1993 Statistical properties of decaying two-dimensional turbulence. *J. Phys. Soc. Japan* **62**, 1193–1202.

OHKITANI, K. 1991 Wave number space dynamics of enstrophy cascade in a forced two-dimensional turbulence. *Phys. Fluids* A **3**, 1598–1611.

RAYLEIGH, LORD 1880 On the stability, or instability, of certain fluid motions. *Proc. Lond. Math. Soc.* **11**, 57–70.

SANTANGELO, P., BENZI, R. & LEGRAS, B. 1989 The generation of vortices in high-resolution, two-dimensional decaying turbulence and the influence of initial conditions on the breaking of similarity. *Phys. Fluids* A **1**, 1027–1034.

SIGGIA, E. D. 1981 Numerical study of small scale intermittency in three dimensional turbulence. *J. Fluid Mech.* **107**, 375–406.

SMITH, L. E. & YAKHOT, V. 1993 Bose condensation and small-scale structure generation in a random force driven two dimensional turbulence. *Phys. Rev. Lett.* **71**, 352–355.